Poly(ionic liquid)–ionic liquid membranes with fluorosulfonyl derived anions: characterization and biohydrogen separation

Andreia S.L. Gouveia,[a,b] Eglè Malcaitè,[a] Elena I. Lozinskaya,[c] Alexander S. Shaplov,[d] Liliana C. Tomé,[e,] and Isabel M. Marrucho[a,b,*]*

[a] Centro de Química Estrutural and Departamento de Engenharia Química, Instituto Superior Técnico, Universidade de Lisboa, Avenida Rovisco Pais, 1049-001 Lisboa, Portugal.

[b] Instituto de Tecnologia Química e Biológica António Xavier, Universidade Nova de Lisboa, Av. da República, 2780-157 Oeiras, Portugal.

[c] A.N. Nesmeyanov Institute of Organoelement Compounds, Russian Academy academy of Sciences sciences (INEOS RAS), Vavilov str. 28, 119991, GSP-1, Moscow, Russia.

[d] Luxembourg Institute of Science and Technology (LIST), 5 avenue des Hauts-Fourneaux, L-4362 Esch-sur-Alzette, Luxembourg.

[e] POLYMAT, University of the Basque Country UPV/EHU, Joxe Mari Korta Center, Avda. Tolosa 72, 20018 Donostia-San Sebastian, Spain.

***Corresponding Authors**

lilianasofi.carvalho@ehu.eus. Tel: +34 943 018018

isabel.marrucho@tecnico.ulisboa.pt. Fax: +351 21 8499242. Tel: +351 21 8413385

ABSTRACT

Clean and sustainable energy production has become a key global issue concerning the world's energy shortage and environmental problematic. Despite the recognized potential of biohydrogen (bioH_2) for sustainable development, there are still issues regarding its production and purification, such as the elimination of CO_2, N_2, and other impurities (H_2O and H_2S), so that an enriched H_2 stream can be obtained for efficient energy generation. The use of poly(ionic liquid)s (PILs) and their derived composite materials incorporating ionic liquids (PIL–IL) has been considered as a highly promising strategy to design membranes with improved CO_2 separation. In this study, membranes of pyrrolidinium-based PILs containing symmetric or asymmetric fluorosulfonyl derived anions, namely bis(fluorosulfonyl)amide ($[FSI]^-$), (trifluoromethyl)sulfonyl-N-cyanoamide ($[TFSAM]^-$) and (trifluoromethyl)sulfonyl-N-trifluoroacetamide ($[TSAC]^-$), were prepared by the incorporation of different amounts of structurally similar ILs. The PIL–IL membranes were characterized by different techniques (TGA, DSC, FT-IR and Raman) and their CO_2/H_2 and H_2/N_2 separation performances were investigated. Higher CO_2/H_2 selectivities were obtained for PIL FSI–40 [C_2mim][FSI] ($\alpha_{CO2/H2}$ = 9.0) and PIL TFSAM–40 [C_2mim][TFSAM] ($\alpha_{CO2/H2}$ = 7.1) compared to those of PIL–IL membranes containing the conventional $[TFSI]^-$ anion at similar or even higher amounts of IL's incorporation.

KEYWORDS

Poly(ionic liquid)s, Ionic Liquids, Fluorosulfonyl derived anions, Asymmetric anions, CO_2/H_2 separation, Membranes.

INTRODUCTION

Considering the enormous potential of H_2 as a clean energy carrier for sustainable development, extensive research into novel H_2 production technologies, especially those from renewable sources, has been conducted. Particularly, bioH_2 production and separation processes have been considered as environmentally friendly, given their non-aggressive operating conditions, close to ambient temperature (30 – 40 ºC) and atmospheric pressure (100 kPa) and hence, less energy consuming compared to chemical or electrochemical processes.[1] In addition, the production of H_2 from organic waste materials using biological processes can also help to minimize the environmental impact and leads to a sustainable resources utilization. However, the elimination of CO_2, N_2 and other impurities (H_2O and H_2S) is still an issue that needs to be solved in order to get an enriched H_2 stream for efficient energy generation.[2]

Ionic liquids (ILs) have been shown to be a successful platform to design novel task-specific materials for CO_2 capture and separation.[3] Supported ionic liquid membranes (SILMs) is the simplest approach to use ILs as gas separation membranes, in which the IL is immobilized into the pores of a solid inert porous membrane.[4] Several works have investigated the effect of the design of chemical structure of ILs on CO_2 separation performance, covering a wide range of cations and anions.[3] In particular, we explored the use of ILs based on 1-ethyl-3-methylimidazolium ($[C_2mim]^+$) cation and several fluorosulfonyl derived anions, such as bis(fluorosulfonyl)imide ($[FSI]^-$), 2,2,2-trifluoromethylsulfonyl-*N*-cyanoamide ($[TFSAM]^-$) and bis[(pentafluoro-ethyl)sulfonyl]imide ($[BETI]^-$). The results showed that both $[C_2mim][TFSAM]$ and $[C_2mim][FSI]$-based SILMs present CO_2/N_2 separation performance above the respective 2008 upper bound.[5] To substitute the expensive and unusual asymmetric $[TFSAM]^-$ anion structure, which combines both fluorinated and cyano functional groups, equimolar IL mixtures

of two structurally similar ILs having common ions, namely [C_2mim][TFSI] and [C_2mim][$N(CN)_2$], were also explored.[5] Although the use of IL mixtures is a promising strategy to tailor gas permeation through SILMs, the pure [C_2mim][TFSAM] provides a SILM with highest CO_2 permeabilities, diffusivities and solubilities compared to those prepared with IL mixtures.[5] Besides, the introduction of asymmetry in the IL anion's chemical structure have also been reported by several authors as an alternative strategy to decrease the viscosity and melting point of ILs.[6-11]

Despite the promising results, the long-term stability and industrial operation of SILMs are still compromised mainly due to the risk of IL draining from pores of the support at high pressures or/and at high temperatures. On the other hand, different studies have been unveiling that the use of poly(ionic liquid)s (PILs) and their composites (PIL–IL) offer an alternative strategy.[3, 12-14] Several studies have been demonstrating that gas permeation properties of the neat IL significantly influence the CO_2 separation performance of PIL–IL composites, consolidating the huge potential of PIL–IL membranes for post-combustion flue gas treatment.[14-19]

However, within the context of CO_2/H_2 separation using PIL–IL membranes, only a restricted number of works have been published in the literature. Briefly, polybenzimidazole-based PILs with asymmetric structure on the imidazolium moiety were synthesized by Kharul *et al.*[20] and CO_2 and H_2 permeabilities both around 30 Barrer were obtained.[20] Carlisle *et al.*[21] explored PIL–IL gel membranes synthesized by photopolymerization of oligo(ethylene glycol)-functionalized crosslinker (difunctional monomer) and vinylimidazolium IL monomers in the presence of [C_2mim][TFSI]. The composite membrane containing 100 mol% of difunctional monomer and 75 wt% of IL revealed CO_2 permeability of 540 Barrer and CO_2/H_2 selectivity of 12 at room temperature. More recently, we studied the CO_2/H_2 separation performance of PIL–IL

membranes prepared with pyrrolidinium-based PILs having fluorinated ($[TFSI]^-$) or cyano-functionalized ($[C(CN)_3]^-$) anions and different amounts of free ILs, at the typical bioH_2 production conditions (T = 35 ºC and 100 kPa of feed pressure).[22] The studied PIL–IL membranes revealed similar or superior CO_2/H_2 separation performance compared to the few PIL–based membranes reported so far,[22] as it is the case of the PIL $C(CN)_3$–60 IL $C(CN)_3$ membrane that displayed CO_2 permeability of 505 Barrer and CO_2/H_2 selectivity of 12.5.

Encouraged by the good results previously obtained for SILMs with asymmetric anions, the film-forming ability of pyrrolidinium-based PILs containing asymmetric ($[TFSAM]^-$ and $[TSAC]^-$) and symmetric ($[FSI]^-$) anions (Figure 1) is herein explored. Several PIL–IL membranes were prepared by the incorporation of different amounts of free IL and, along with both neat PIL and IL components, were characterized using different techniques, such as TGA, DSC and FT-IR/Raman spectroscopies. Furthermore, the CO_2, N_2 and H_2 permeation properties were evaluated using the time-lag method at biohydrogen production conditions (T = 35ºC and 100 kPa of feed pressure) and the effect of introducing asymmetry in both PIL and IL anion's structures on CO_2/H_2 and H_2/N_2 separation performances was investigated.

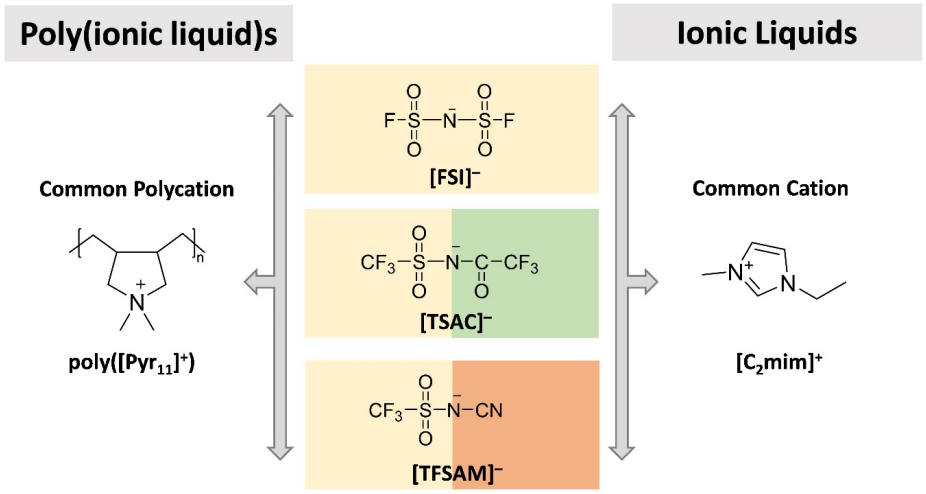

Figure 1. Chemical structures of the PILs and ILs used in this work.

EXPERIMENTAL SECTION

Materials.

Poly(diallyldimethylammonium) chloride (poly([Pyr_{11}][Cl])) solution (average M_w 400,000 – 500,000, 20 wt% in water, Aldrich), acetone (Aldrich, 99.8%), dimethyl sulfoxide (DMSO, TCI Chemicals, > 99.7%) and potassium bis(fluorosulfonyl)imide (KFSI, Fisher Scientific, > 95%) were used as received. 1-Ethyl-3-methylimidazolium bis(fluorosulfonyl)imide ([C_2mim][FSI], 99.5%) was provided by Solvionic. Carbon dioxide (CO_2), nitrogen (N_2) and hydrogen (H_2) were supplied by Air Liquide with a minimum purity of 99.99%. Potassium 2,2,2-trifluoromethylsulfonyl-*N*-cyanoamide (KTFSAM) was synthesized in accordance with the procedure published by our group previously[6] (for details see the Supporting Information (SI) file). Potassium 2,2,2-trifluoro-*N*-(trifluoromethylsulfonyl) acetamide (KTSAC) was prepared following general procedure reported by Matsumoto H. et al.[9] (see SI file). Ionic liquids, 1-ethyl-3-methylimidazolium 2,2,2-trifluoromethylsulfonyl-*N*-cyanoamide ([C_2mim][TFSAM], 98.5–99.0%) and 1-ethyl-3-methylimidazolium 2,2,2-trifluoro-*N*-(trifluoromethylsulfonyl) acetamide

([C_2mim][TSAC], 98 %) were synthesized according to a previously described procedure.[6, 5, 23] Poly([Pyr_{11}][FSI]), poly([Pyr_{11}][TFSAM]) and poly([Pyr_{11}][TSAC]) PILs were synthesized by anion metathesis reactions from the commercially available precursor, poly([Pyr_{11}][Cl]), according to previously established procedures.[14, 24, 25] All salts, ILs and PILs were characterized by elemental analysis, NMR and IR spectroscopy, which was in accordance with those reported in the literature.[6, 9, 14, 24-26]

Synthesis of [Pyr_{11}][TSAC]

In the case of poly([Pyr_{11}][TSAC]), here reported for the first time, a solution of 8.43 g (28.58 mmol) of KTSAC salt in 10 mL of double-distilled water was added to a solution of 4.4 g (27.22 mmol of monomeric units) of poly([Pyr_{11}][Cl]) in 110 mL of water and the mixture was stirred for 30 min at room temperature. The precipitated polymer was thoroughly washed with excess of water, filtered and dried in vacuum at 45ºC and 133 Pa until constant weight was attained. Yield: 7.76 g (77%). ^{1}H NMR (400 MHz, DMSO-d_6): 3.72 (br. m, 2H, NCH_2, *pseudo e*), 3.35-3.10 (m, 5H, NCH_2, *pseudo a,* CH_3 *pseudo e*), 3.08 (m, 3H, CH_3 *pseudo a*), 2.53-2.50 (m, 1.7H, *cis*-C^3H-C^4H), 2.09 (m, 0.3H, *trans*-C^3H-C^4H), 1.54-1.02 (br. m, 4H, CH_2-CH_2); ^{13}C NMR (100.6 MHz, DMSO-d_6): 160.1 (CO), 124.9-115.3 (q, $^1J_{CF}$ = 322 Hz, $\underline{C}F_3SO_2$), 121.2-112.6 (q, $^1J_{CF}$ = 290 Hz, CO$\underline{C}F_3$), 69.5, 53.1, 51.3, 37.9, 37.3, 26.5. ^{19}F NMR (376.5 MHz, DMSO-d_6, C_6F_6): -74.4 (s, COC$\underline{F}_3$), -77.9 (s, $SO_2C\underline{F}_3$). IR (ATR-mode): 2948 (w, ν_{C-H}), 287 (w, ν_{C-H}), 1670 (s, $\nu_{C=O}$), 1475 (m), 1433 (w), 1317 (s, ν_{asSO2}), 1213 (w, ν_{CF}), 1167 (vs, ν_{sSO2}), 1120 (vs, ν_{CF}), 918 (m), 823 (s), 760 (m), 620 (s), 592 (s), 544 (m) cm^{-1}.

Considering the different hygroscopic properties of each anion, in the case of $[FSI]^-$ anion, the poly([Pyr_{11}][FSI]) was obtained as a white powder, while for $[TFSAM]^-$ and $[TSAC]^-$ anions with asymmetric structures, PILs represented highly sticky solids after precise drying.

Preparation of PIL–IL membranes

Dense composite membranes based on the synthesized PILs and defined quantities of imidazolium ILs having identical anions were prepared by solvent casting (Figure 2). Firstly, 6 (wt/v)% solutions of poly([Pyr_{11}][FSI]), poly([Pyr_{11}][TFSAM]) and poly([Pyr_{11}][TSAC]) in appropriate solvent were prepared and then the respective IL amounts were added (Table 1). The solutions were stirred until complete dissolution of all components at room temperature whereupon were poured into the glass Petri dishes and left for slow evaporation of the solvent. Depending on the solvent used, the evaporation time and temperature of the casting process were optimized for each case and details of the procedure are listed in Table 1. The obtained membranes were taken carefully out of the Petri dishes and were finally dried at 50 ºC and 133 Pa for 12 h.

The thicknesses of the prepared membranes (105–285 μm) were measured using a digital micrometer (Mitutoyo, model MDE-25PJ, Japan). At this, the thickness used in calculation of gas permeabilities and diffusivities was taken as an average from six measurements performed at different membrane locations.

Table 1. Composition descriptions and experimental conditions of the casting procedure used to prepare the PIL–IL membranes.

PIL-IL membrane	Polymer (PIL)	Ionic Liquid (IL)	wt% of IL	Solvent	*T* (ºC)	Evaporation time (days)
PIL FSI – 20 IL FSI	Poly([Pyr_{11}][FSI])	[C_2mim][FSI]	20	DMSO	50	4
PIL FSI – 40 IL FSI			40			
PIL TFSAM – 20 IL TFSAM	Poly([Pyr_{11}][TFSAM])	[C_2mim][TFSAM]	20	Acetone	25	3
PIL TFSAM – 40 IL TFSAM			40			
PIL TSAC – 20 IL TSAC	Poly([Pyr_{11}][TSAC])	[C_2mim][TSAC]	20	Acetone	25	3

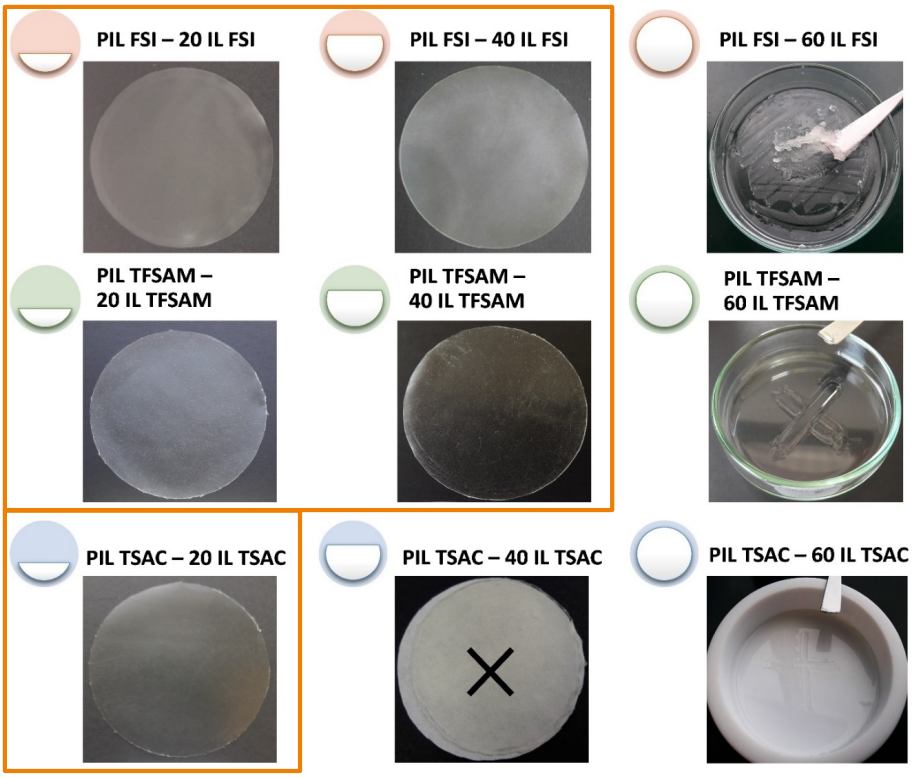

Figure 2. Images of the prepared PIL–IL composite membranes with different amounts of IL (successful (□) and unsuccessful cases).

Characterization

FT-IR spectra were acquired using a Thermo Electron Corporation Nicolet 5700 spectrometer with a DTGS-TEC detector. The spectra were registered using a diamond ATR Smart Orbit™ accessory and collected using 128 scans, from 500 to 4000 cm^{-1}, with a resolution of 4 cm^{-1}.

Raman spectra were measured using a LabRAM HR 800 Evolution Horiba–Jobin Yvon confocal micro-Raman spectrometer, with a diffraction grating of 600 gr/mm at a spectral resolution of 4 cm^{-1}. The excitation source was a 532 nm (or a 785 nm in the case of PIL–20 IL TSAC membrane) diode laser with ~10 mW power on the sample. The objective used was x50 (LWD) and the spectra were acquired with 10 s of signal collection time and four accumulations. Although all bands in the Raman spectra were well-defined using the 532nm laser, a slight fluorescence effect can be observed in some of the collected Raman spectra considering that fluorescence background is a known issue in Raman spectroscopy of ILs.[27]

NMR spectra were recorded on AMX-400 and Avance II 500 MHz spectrometers (Bruker) at 25 °C in the indicated deuterated solvents and are listed in ppm. The signal corresponding to the residual protons of the deuterated solvent was used as an internal standard for ^{1}H and ^{13}C NMR, while the C_6F_6 was utilized as an external standard for ^{19}F NMR.

Thermogravimetric analysis (TGA) was performed on a TGA Q50 analyzer (TA Instruments) under nitrogen atmosphere. All the samples were dried under vacuum (1 Pa) at a moderate temperature (≈ 45 ºC) for at least 2 days before measurements. In the case of neat PILs and the PIL–IL composites, TGA experiments were performed at a heating rate of 10 ºC min^{-1} from room temperature to 800 ºC, while for neat ILs, the TGA experiments were only performed until 600 ºC since open aluminum pans were used to support the liquid samples.

A Q200 differential scanning calorimeter (TA Instruments) was used to perform the DSC experiments. All the samples were dried under vacuum (1 Pa) at a moderate temperature (≈ 45

ºC) for at least 2 days before measurements. Then, the samples were weighed (~9–12 mg) with the precision of ± 0.0001 g and hermetically sealed in aluminum pans under inert atmosphere inside an argon-filled glovebox (MBRAUN MB-Labstar, H_2O and O_2 content <0.5 ppm).

The DSC experiments for neat PILs and PIL–IL membranes were carried out at a heating rate of 10 ºC min^{-1} in a large temperature window, from –90 to 200 ºC, in order to obtain a broader insight of their thermal profiles. Crystallization (T_c) and melting (T_m) points were determined as extrapolated onset temperatures. For all measurements, a first cycle was always performed to eliminate the thermal history of each sample. In the case of neat IL samples, both crystallization and melting temperatures were taken from Shaplov et al.[6] which were performed at a heating rate of 2 ºC min^{-1} as recommended for an extra accurate measurement of ILs thermal properties.[28, 29]

Gas Permeation Experiments

Ideal CO_2, N_2 and H_2 permeabilities and diffusivities were measured using a time-lag equipment, described in detail elsewhere.[19] Each membrane was degassed under vacuum inside the permeation cell during at least 12 h before testing. The gas permeation measurements were performed at 35 ºC with an upstream pressure of 100 kPa (feed) and vacuum (< 0.1 kPa) as the initial downstream pressure (permeate). Three separate CO_2, N_2 and H_2 experiments on each duplicate PIL–IL membrane sample were carried out to ensure accuracy. The reported gas permeation data are the average values, in which the highest relative precision was 0.047 for gas permeabilities, 0.098 for gas diffusivities and 0.068 for gas solubility values.

The gas transport through PIL–IL membranes was assumed to occur according to solution-diffusion mass transfer mechanism.[30] Thus, the permeability (P) is related to diffusivity (D) and solubility (S) as follows:

$$P = D \times S \quad (1)$$

The permeate flux of each studied gas (J_i) was determined using Eq. (2), assuming an ideal gas behavior and a homogeneous membrane.[31]

$$J_i = \frac{V^p \Delta p_d}{AtRT} \quad (2)$$

where V^p is the permeate volume, Δp_d is the variation of downstream pressure, A is the effective membrane surface area, t is the experimental time, R is the Gas Constant and T is the temperature. Ideal gas permeability (P_i) was then calculated from the pressure driving force (Δp_i) and membrane thickness (ℓ) as shown in Eq. (3).

$$P_i = \frac{J_i}{\Delta_{pi}/\ell} \quad (3)$$

Eq. (4) was used to determine gas diffusivity (D_i). The time-lag parameter (θ) was deduced by extrapolating the slope of the linear portion of the p_d vs. t curve back to the time axis, where the intercept is equal to θ.[32]

$$D_i = \frac{\ell^2}{6\theta} \quad (4)$$

Gas solubility (S_i) was calculated using the relationship given by Eq. (1), after defining both P_i and D_i.

The ideal permeability selectivity (or permselectivity), $\alpha_{i/j}$, which can also be expressed as the product of diffusivity selectivity and solubility selectivity, was obtained by dividing the permeability of the more permeable specie i to the permeability of the less permeable specie j, as described in Eq. (5).

$$\alpha_{i/j} = \frac{P_i}{P_j} = \left(\frac{D_i}{D_j}\right) \times \left(\frac{S_i}{S_j}\right) \quad (5)$$

RESULTS AND DISCUSSION

Characterization of PILs and ILs.

Fourier-Transform Infrared (FT-IR) Spectroscopy.

FT-IR spectroscopy was performed to confirm the chemical structure of the synthesized PIL and IL components containing different fluorosulfonyl anions, as well to evaluate possible interactions between the different components in the prepared membranes. The obtained FT-IR spectra of the PILs, ILs and their respective PIL–IL membranes are depicted in Figures 3a – 3c). Considering the asymmetric nature of $[TFSAM]^-$ and $[TSAC]^-$ anions, presenting in their anion's structure half of the conventional $[TFSI]^-$ anion structure, both PIL and IL components incorporating the latter anion, are also shown in Figure 3d). Bearing in mind that ILs used in this work have a common imidazolium cation ($[C_2mim]^+$) in their structure, the most characteristic absorption bands of the imidazolium ring can be seen in Figures 3a – 3d) at around 3120-3126 cm^{-1} and 3157-3163 cm^{-1} attributed to C–H stretching modes of the imidazolium ring and at around 1574 cm^{-1}, assigned to ring in-plane symmetric/asymmetric stretch and $–CH_2(N)/–CH_3(N)CN$ stretch.[33-36] Likewise, considering that pyrrolidinium polycation ($[Pyr_{11}]^+$) is common to all studied PILs, the absorption bands detected at 2939-2962 cm^{-1} and 2871-2875 cm^{-1} are associated to $–CH_2$ stretching vibrations, while the bands observed at around 1475 cm^{-1} are assigned to the $–CH_3$ bending vibration originated from the pendant methyl units of the cationic backbone (Figures 3a–3d).

Figure 3a displays the FT-IR spectra of both PIL and IL containing the $[FSI]^-$ anion and corresponding PIL–IL membranes. The absorption bands observed at 1377 and 1359 cm^{-1} are attributed to $–SO_2$ asymmetric stretching, while the band at 1166 cm^{-1} is assigned to $–SO_2$

symmetric stretching.[37-39] Two other peaks at 827 and 727 cm^{-1}, respectively associated with S–N–S asymmetric and symmetric stretching,[37, 38] are also observed in both [C_2mim][FSI] and poly([Pyr_{11}][FSI]) spectra.

In what concerns PIL, IL and PIL–IL membranes containing $[TFSAM]^-$ anion, which has an asymmetric chemical structure (Figure 1), from Figure 3b, the strong –CN stretching vibration at 2187 cm^{-1} as well as the vibrational bands at 1326 cm^{-1} ($–SO_2$ asymmetric stretching), 1213 cm^{-1} ($–CF_3$ stretching modes), 1164 cm^{-1} ($–SO_2$ symmetric stretching) and 1114 cm^{-1} ($–CF_3$ stretching modes) are clearly observed attributing to cyano and trifluoromethylsulfonyl functional groups, respectively. This infrared pattern obtained is similar to those previously published by Shaplov et al.[6] for other ILs containing the $[TFSAM]^-$ anion.

Figure 3c shows the FT-IR spectra of the compounds bearing the asymmetric $[TSAC]^-$ anion. The characteristic absorption bands of the $[TSAC]^-$ anion appear at 1670 cm^{-1} (–C=O stretching vibration), 1317 cm^{-1} ($–SO_2$ asymmetric stretching), 1120 and 1213 ($–CF_3$ asymmetric stretching) and at 1167 cm^{-1} ($–SO_2$ symmetric stretching). Two more peaks, detected at 918 and 823 cm^{-1}, with low to medium intensity, might also be assigned to $[TSAC]^-$ anion, since they appear in both PIL and IL spectra. It should be mentioned that no literature data was found related to FT-IR spectroscopy analysis of PILs or ILs containing the $[TSAC]^-$ anion. From Figure 3d, the partial similarity of the $[TFSI]^-$ anion structure compared to the $[TFSAM]^-$ and $[TSAC]^-$ anion structures can be confirmed by the characteristic bands of $–CF_3$ or $–SO_2$ functional groups present in each respective spectrum.

Furthermore, from Figures 3a – 3c, all the characteristic absorption bands assigned to different anions and cations in ILs and PILs can be found in the FT-IR spectra of the respective PIL–IL membranes. Depending on the amount of IL incorporated in the membranes, the

differences in intensity of the bands associated with both imidazolium cation and pyrrolidinium polycation were observed. Finally, no significant deviations were observed in the PIL–IL membranes FT-IR spectra in comparison with the spectra of the respective neat components, even by increasing the amount of IL in the composite membranes.

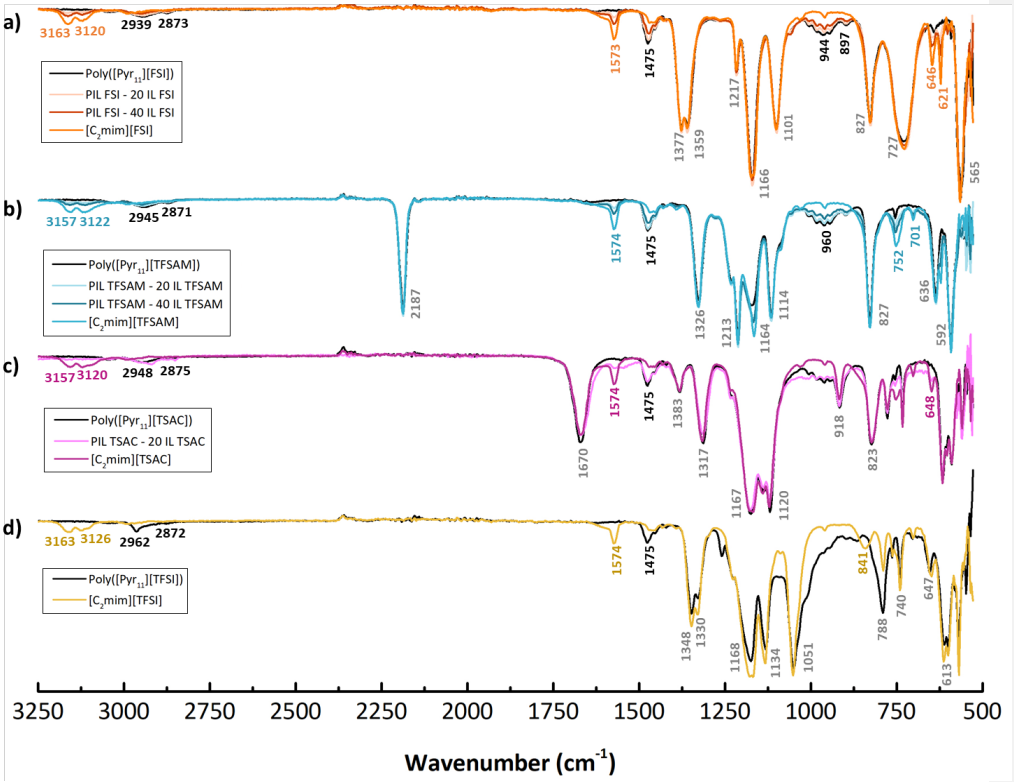

Figure 3. FT-IR spectra of both neat PILs and ILs and respective PIL–IL membranes bearing different anions: (a) $[FSI]^-$, (b) $[TFSAM]^-$; (c) $[TSAC]^-$ and (d) $[TFSI]^-$.

Raman Spectroscopy.

Raman spectroscopy was also used to analyze the chemical structure of the synthesized PIL and IL samples and possible PIL–IL interactions as a complementary technique to FT-IR spectroscopy. Depending of the vibrational modes of each sample, some of the bands show high

intensity in FT-IR spectra and low intensity in Raman spectra or vice-versa. In addition, considering that Raman spectroscopy can provide information at lower wavenumbers (< 400 cm^{-1}) compared to FT-IR spectroscopy, a wide spectrum range can also be evaluated.

The Raman spectra of PILs and ILs bearing $[TFSAM]^-$, $[FSI]^-$ and $[TSAC]^-$ anions and respective PIL–IL membranes are provided in Figures S1 – S3 (see Supporting Information file). It should be mentioned that, to the best of our knowledge, no literature data has been yet published describing the analysis of ILs or PILs with $[TFSAM]^-$ or $[TSAC]^-$ asymmetric anions by Raman spectroscopy.

PIL and IL structures containing $[TFSAM]^-$ (Figure S1)) and $[TSAC]^-$ (Figure S3) anions show the characteristic bands at 2186 cm^{-1} (–CN stretching vibration) and at 1670 cm^{-1} (–C=O stretching vibration). The other pronounced bands were found at 1320 cm^{-1} ($–SO_2$ asymmetric stretching), 1170 cm^{-1} ($–SO_2$ symmetric stretching) 1213 and 1120 cm^{-1} ($–CF_3$ asymmetric stretching). At low wavenumbers, three well-defined bands attributed to the $[TFSAM]^-$ anion structure at around 162 cm^{-1} ($–CF_3$ torsion vibration), 301 cm^{-1} ($–CF_3$ bending vibration) and 335 cm^{-1} ($–SO_2$ torsion vibration) can be observed in Figure S1. These assignments were also reported for ILs containing the $[TFSI]^-$ anion, having similar CF_3SO_2- group.[36] Two more bands at 447 and 478 cm^{-1} are simultaneously visible in $[C_2mim][TFSAM]$, poly($[Pyr_{11}][TFSAM]$) and composite membranes spectra, which means that they can also be attributed to the $[TFSAM]^-$ anion. The intensities of the described vibrational modes were found to be different for $[C_2mim][TFSAM]$ and poly($[Pyr_{11}][TFSAM]$), that can be explained by the specific interactions between $[TFSAM]^-$ anion and imidazolium or pyrrolidinium cations (Figure S1).[40] However, no frequency shift or change in the appearance of specific vibrational modes were detected in Figure S1c.

For [C_2mim][TSAC], poly([Pyr_{11}][TSAC]) and composite membrane on their basis three absorption bands at 263 (–CF_3 bending vibration),[41] 309 (–CF_3 bending vibration) and 404 cm^{-1} (–SO_2 wagging vibration) can be observed (Figure S3).[36] Additionally, one more absorption band with slightly higher intensity can also be seen at 223 cm^{-1}, which is probably associated to the $[TSAC]^-$ anion, since it appears in all PIL, IL and PIL–IL membrane's spectra.

Figure S2 shows Raman spectra of [C_2mim][FSI], poly([Pyr_{11}][FSI]) and their composites with 20 and 40 wt% of IL. Correspondingly to what was observed in FT-IR analysis, the characteristic bands of $[FSI]^-$ anion in Raman spectra appear at 1361 (SO_2 asymmetric stretching), 1215 (SO_2 symmetric stretching), 828 (SNS asymmetric stretching) and at 725 cm^{-1} (SNS symmetric stretching). In addition, at low wavenumbers, the –SO_2F torsion vibrational mode can be found at 289 cm^{-1} in all the studied spectra, as well as the –SO_2F bending vibrational modes can be seen at 324, 356, 452 and 481 cm^{-1}. All these assignments were found to be in agreement with the previously reported data.[36, 38]

Overall, some differences in the intensity of the bands in the Raman spectral region of 50 – 400 cm^{-1} for all ILs, PILs and PIL–IL membranes were observed, that can be attributed to the different anion-cation interactions.[40] In addition, similarly to what was observed in FT-IR analysis, no band shifts were observed in Raman spectra with increasing amount of ILs in all composite membranes.

Thermogravimetric analysis.

The degradation profiles of PILs, ILs and PIL–IL membranes were assessed by TGA analysis, not only to determine their onset decomposition temperatures, but also to study the influence of the IL content on the thermal stability of the prepared membranes. Both onset (T_{onset}) and

decomposition (T_d) temperatures are given in Table 2, while the TGA thermograms are provided in Figure S4 for neat ILs, Figure S5 for neat PILs and in Figures S6 – S8 for PIL–IL membranes.

Thermal stability of ILs with respect to counter anion structure was found to be evolved as follows (Table 2): T_{onset} [C_2mim][TSAC] 295 ^oC > T_{onset} [C_2mim][TFSAM] 250 ^oC > T_{onset} [C_2mim][TFSAM] 215 ^oC. At the same time for PILs, the transition from $[FSI]^-$ to $[TSAC]^-$ and further to $[TFSAM]^-$ anions affords an increase in their thermal stability following the following order (Table 2): T_{onset} poly([Pyr_{11}][TFSAM]) 280 $^oC \geq T_{onset}$ poly([Pyr_{11}][TSAC) 270 ^oC > T_{onset} poly([Pyr_{11}][FSI]) 220 ^oC. Both neat ILs and PILs displayed single weight-loss step degradation profile (Figures S4 and S5, respectively), being the PIL containing the $[FSI]^-$ anion the only exception with two degradation steps, at 220 and ~260 ºC. In the case of TSAC system, the T_{onset} of imidazolium IL was higher than the one of pyrrolidinium PIL, while the comparison of PIL–IL composites bearing $[TFSAM]^-$ and $[FSI]^-$ anions revealed the opposite dependence (Table 2). This can be explained by the fact that independently of the cation nature the thermal stability of polycations is usually higher than that of structurally similar ILs.[42]

Regarding PIL–IL membranes, their thermal stability varies in between the T_{onset} values of respective ILs and PILs. The incorporation of $[FSI]^-$ and $[TFSAM]^-$ containing imidazolium ILs into the corresponding PILs reduces the thermal stability of membranes in comparison with neat PILs (Table 2). In contrast, the T_{onset} of membranes with $[TSAC]^-$ anion does not change after the incorporation of 20 wt% of neat IL. From the Figures S6 – S8, it can also be perceived that the PIL–IL membranes generally follow the thermal profile of the respective neat PILs, probably due to the fact that the polymer fraction dominates the composition. Summarizing the data reported in Table 2, it can be concluded that all PIL–IL membranes are thermally stable up to 200 ^oC making them attractive as materials for gas separation membranes.

Table 2. Thermal properties of studied PILs, ILs and PIL–IL membranes: onset (T_{onset}), crystallization (T_c), melting (T_m) and glass transition (T_g) temperatures.

Sample	T_{onset} (°C)[a]	T_c (°C)[b]	T_m (°C)[b]	T_g (°C)[c]
PIL poly([Pyr_{11}][FSI])	220	-	-	-
PIL FSI – 20 IL FSI	215	-	-	-
PIL FSI – 40 IL FSI	210	-	-	-
[C_2mim][FSI]	215	-30	-16	-
PIL poly([Pyr_{11}][TFSAM])	280	-	-	51
PIL TFSAM – 20 IL TFSAM	255	-	-	-24
PIL TFSAM – 40 IL TFSAM	250	-	-	-23
[C_2mim][TFSAM]	250	-54	-22	-
PIL poly([Pyr_{11}][TSAC])	270	-	-	23
PIL TSAC – 20 IL TSAC	270	-	-	-7
[C_2mim][TSAC]	295	-40	-10	-

[a] T_{onset} defined as the onset weight loss of the sample by TGA.
[b] Taken from Shaplov et al.[6]
[c] Determined by DSC.

Differential scanning calorimetry.

The neat PILs, ILs and respective PIL–IL membranes were also characterized by DSC analysis. The determined melting (T_m), crystallization (T_c) and glass transition (T_g) temperatures

Alexzip 24/12/19 16:23
Eliminado: Salto de sección (Continua)

are listed in Table 2, while the DSC curves of neat PILs and PIL–IL composites are provided on Figures S9 – S12 (see the ESI file).

From Shaplov et al.[6] all neat ILs showed both crystallization and melting temperatures. For instance, [C_2mim][FSI] revealed T_c peak around –30 ºC, as well as T_m at –16 ºC and no T_g was detected. Similarly, ILs containing asymmetric anions such as [C_2mim][TFSAM] and [C_2mim][TSAC], showed only T_c and T_m temperatures (Table 2). At this, both transitions occur at lower temperatures than that of [C_2mim][FSI] proving the statement that asymmetry of anions are playing an important role in the synthesis of low melting salts.[7, 28, 32]

Analyzing the DSC results of the neat PILs (Table 2 and Figure S9), it can be seen that no obvious T_g was detected for poly([Pyr_{11}][FSI]). This finding is in accordance with previously reported results for similar PILs.[37, 43] Conversely, well-defined glass transition temperatures were observed at 51 and 23 ºC for the PILs bearing asymmetric $[TFSAM]^-$ and $[TSAC]^-$ anions, respectively.

Similarly to neat poly([Pyr_{11}][FSI]), the PIL–IL membranes with 20 and 40 wt% of [C_2mim][FSI] IL display no T_g values In contrast, the T_g values of PIL–IL membranes with $[TFSAM]^-$ and $[TSAC]^-$ anions are significantly lower than those of respective neat PILs (Table 2 and Figures S10 and S12). The reduction in T_g is more significant for the PIL–IL TFSAM membranes, indicating a stronger plasticizing effect of the [C_2mim][TFSAM] IL within the PIL polymer chains. On the other hand, the T_g values of PIL–IL TFSAM membranes do not significantly change when increasing the amount of free IL from 20 to 40 wt%. The observed tendency slightly differs from what has been reported in literature,[44-46] which is the reduction of Tg when increasing the IL content into polymer matrices.

Gas Permeability, Diffusivity and Solubility of PIL-IL membranes.

The measured CO_2, N_2 and H_2 permeabilities (*P*) and diffusivities (*D*) of the prepared PIL–IL membranes are presented in Figures 4a and 4b, respectively, while gas solubility (*S*) values calculated using Eq. (1) are shown in Figure 4c.

The same trend of gas permeabilities was obtained for all studied PIL–IL membranes: $PCO_2 >> PH_2 > PN_2$ (Figure 4a). The CO_2, N_2 and H_2 permeabilities increase with the amount of IL incorporated into the composites. For instance, in the case of PIL–IL FSI membranes, the increment of IL (from 20 to 40 wt%) led to 5.5, 4 and 2 times increase in CO_2, N_2 and H_2 permeabilities, respectively. Comparison of CO_2 permeabilities for PIL–IL composites containing 20 wt% of IL revealed the following order (Figure 4a): PIL–20 IL TSAC (72) > PIL–20 IL TFSAM (40) ≈ PIL–20 IL FSI (38 Barrer). However, this order changed when the amount of the incorporated IL was increased to 40 wt%: PIL–40 IL FSI (201) > PIL–40 IL TFSAM (177 Barrer).

The overall evolution of gas permeabilities for PIL–IL membranes comprising 20 wt% of IL according to anion structure can be summarized as follows: [TSAC] > [TFSAM] > [FSI] (Figure 4a). Unfortunately, for PIL–IL TSAC membranes, it was not possible to prepare mechanically stable and homogeneous membranes at $[C_2mim][TSAC]$ content higher than 20 wt% (Figure 2). This observation indicates that the film-forming ability of PIL–IL materials is strongly dependent on the anion's nature.

Figure 4b displays the experimental CO_2, N_2 and H_2 diffusivities obtained through the prepared composites. Mainly because of the smaller kinetic diameter of H_2 (2.89 Å) compared to that of CO_2 (3.30 Å), the difference of one or two orders of magnitude between H_2 and CO_2

diffusivities was observed.[47] Similarly, the higher N_2 kinetic diameter (3.64 Å) compared to that of H_2 explain the one order of magnitude lower N_2 diffusivities compared to those of H_2. The composite membranes in accordance with the values of the displayed CO_2 and N_2 diffusivities can be ordered as follows: PIL TFSAM–20 IL TFSAM < PIL FSI–20 IL FSI < PIL TSAC–20 IL TSAC < PIL TFSAM–40 IL TFSAM < PIL FSI–40 IL FSI. In fact, the presence of the $[FSI]^-$ anion leads to higher CO_2 and N_2 diffusivities compared to those of the membranes containing the $[TFSAM]^-$ anion. Conversely, a different trend was observed for H_2 diffusivity values: PIL FSI–20 IL FSI < PIL TFSAM–20 IL TFSAM < PIL FSI–40 IL FSI < PIL TSAC–20 IL TSAC < PIL TFSAM–40 IL TFSAM. This means that the presence of a cyano functional group in the $[TFSAM]^-$ anion's structure promotes enhanced H_2 diffusivities when compared to the membranes with 20 and 40 wt% of $[C_2mim][FSI]$. It is also interesting to point out that the membrane prepared with 20 wt% of $[C_2mim][TSAC]$, which has a carbonyl group in its anion, displayed the highest CO_2, N_2 and H_2 diffusivities compared to those of the other PIL–20 IL membranes (Figure 4b).

As it can be seen from Figures 4a and 4b, the CO_2 permeability followed the same trend as CO_2 diffusivity, except for the cases of PIL FSI–20 IL FSI and PIL TFSAM–20 IL TFSAM composites. Similarly, the H_2 permeability followed the same behavior as H_2 diffusivity, except for the case of PIL TSAC–20 IL TSAC membrane, that presents higher H_2 diffusivity compared to PIL FSI–40 IL FSI composite, but lower H_2 permeability. The membranes having 40 wt% IL content showed the highest H_2 permeabilities (177 – 201 Barrer) and diffusivities (1021 – 873 x 10^{-12} m^2 s^{-1}). Furthermore, the superior H_2 diffusivity obtained for PIL TSAC–20 IL TSAC (907 x 10^{-12} m^2 s^{-1}) compared to PIL FSI–40 IL FSI (873 x 10^{-12} m^2 s^{-1}) membrane (Figure 4b) led to

the conclusion that the presence of a carbonyl group in the IL anions' structure has a significant effect on H_2 diffusivity.

As illustrated in Figure 4c, the CO_2 solubility of the prepared PIL–IL membranes ranged from 10.4 to 17.1 (x 10^{-6}) m^3(STP) m^{-3} Pa^{-1}. On the other hand, the N_2 and H_2 solubility values were two orders of magnitude lower, varying from 0.16 and 0.43 (x 10^{-6}) m^3(STP) m^{-3} Pa^{-1} in the case of N_2, and from 0.15 to 0.2 (x 10^{-6}) m^3(STP) m^{-3} Pa^{-1}, in the case of H_2. In addition, improved CO_2 solubilities were obtained by increasing the IL amount incorporated into the membrane. For instance, when increasing the IL content from 20 to 40 wt% into PIL–IL TFSAM membranes, the increment in CO_2 solubility reached 29%. Moreover, this effect was more pronounced for PIL–IL FSI membranes, where the CO_2 solubility increased approximately 63%. A similar behaviour, although less expressed, was also observed for H_2 solubilities. This large difference between CO_2 and H_2 solubilities has also been identified and discussed in our previous study for other PIL–IL membranes.[22] At 20 wt% of IL content, the highest CO_2, N_2 and H_2 solubilities were demonstrated by the membranes with $[TSAC]^-$ asymmetric anion (Figure 4c), similarly to what was observed for gas permeability (Figure 4a) and diffusivity (Figure 4b). Increasing IL content up to 40 wt% the PIL TFSAM–40 IL TFSAM membrane presented the highest CO_2 solubility, while the highest H_2 solubility was observed for PIL FSI–40 IL FSI composite (Figure 4c). Overall, the large difference of H_2 diffusivities compared to CO_2 and N_2 diffusivities is somehow compensated by the very low H_2 solubilities, which significantly impact the H_2 permeability results.

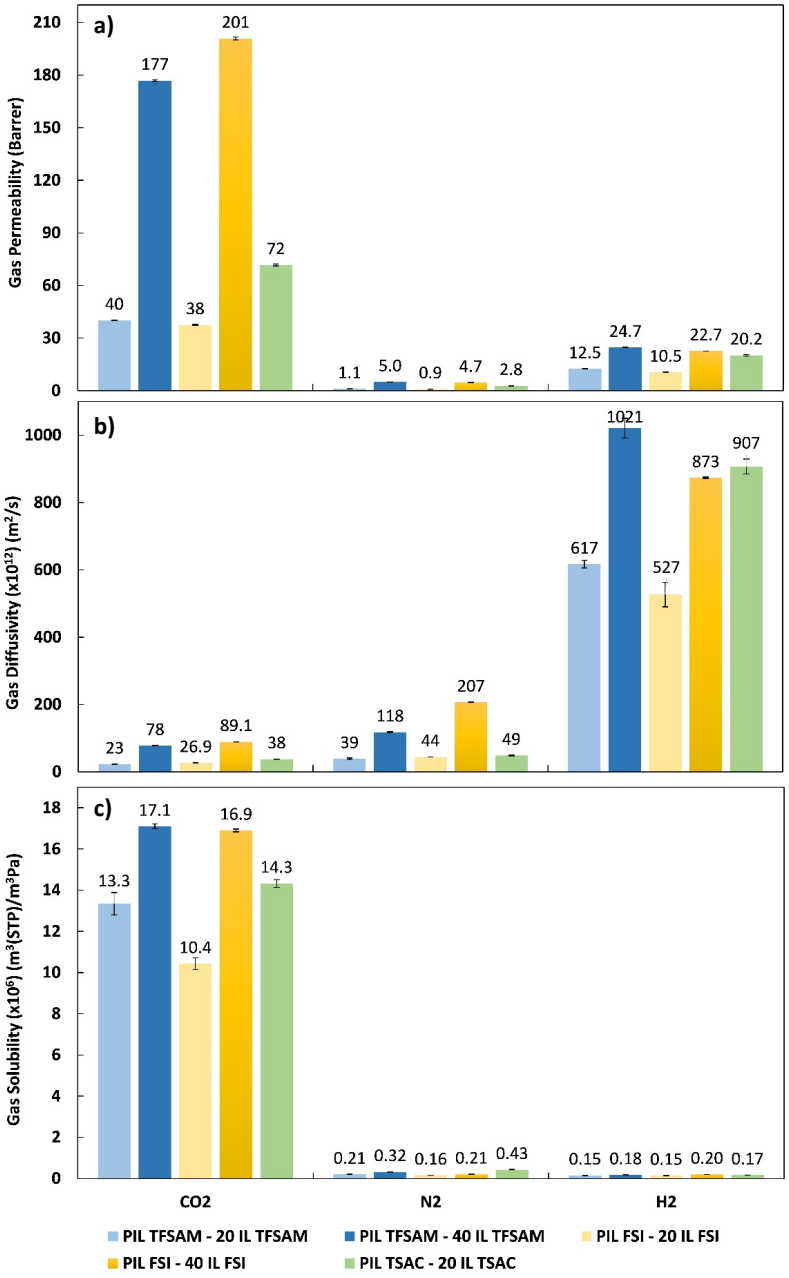

Figure 4. (a) Gas permeabilities (*P*), (b) diffusivities *(D*) and (c) solubilities (*S*) for the studied PIL–IL membranes at T = 35 ºC. Error bars represent standard deviations based on three experimental replicas. In some cases, the standard deviations are very small leading to error bars that cannot be clearly represented.

CO_2/H_2 Separation Performance.

The single CO_2, N_2 and H_2 permeabilities and the ideal CO_2/H_2 and H_2/N_2 selectivities determined at 35 ºC are listed in Table 3. The PIL–IL membranes with 40 wt% of IL exhibited higher CO_2/H_2 and lower H_2/N_2 permselectivities compared to those of the membranes with 20 wt%. For instance, the PIL FSI–40 IL FSI showed higher CO_2/H_2 permselectivity ($\alpha_{CO2/H2} = 8.9$) in comparison with PIL TFSAM–40 IL TFSAM ($\alpha_{CO2/H2} = 7.2$). However, both membranes displayed similar H_2/N_2 permselectivities (~ 5.0). Although the highest CO_2 and H_2 permeabilities were obtained for the PIL TSAC–20 IL TSAC membranes (among those with 20 wt% of IL), the CO_2/H_2 selectivity was found to be nearly independent on the nature of the anion (Table 3).

Table 3. Single gas permeabilities (P)[a] and ideal selectivities (α) of the studied PIL–IL membranes.[b]

PIL-IL membrane	Gas Permeability (Barrer)			Ideal Selectivities	
	$P_{CO2} \pm \sigma$	$P_{N2} \pm \sigma$	$P_{H2} \pm \sigma$	α CO_2/H_2	α H_2/N_2
PIL TFSAM–20 IL TFSAM	40 ± 0.2	1.1 ± 0.02	12.4 ± 0.10	3.2 ± 0.04	11.5 ± 0.22
PIL TFSAM–40 IL TFSAM	177 ± 0.5	5.0 ± 0.01	24.6 ± 0.14	7.2 ± 0.06	4.9 ± 0.06
PIL FSI–20 IL FSI	37 ± 0.3	0.9 ± 0.01	10.5 ± 0.22	3.6 ± 0.10	11.7 ± 0.18
PIL FSI–40 IL FSI	201 ± 0.8	4.5 ± 0.01	22.7 ± 0.10	8.9 ± 0.07	5.0 ± 0.01
PIL TSAC–20 IL TSAC	72 ± 0.6	2.8 ± 0.01	20.2 ± 0.43	3.5 ± 0.11	7.3 ± 0.19

[a] Barrer (1 Barrer = 10^{-10} cm(STP)^3·cm·cm^{-2}·s^{-1}·cm·Hg^{-1}).
[b] The listed uncertainties represent the standard deviations (σ) based on six experiments.

Figure 5 shows the gas separation performance of the studied PIL–IL membranes, in which the CO_2/H_2 permselectivity is plotted against the permeability of the more permeable gas (CO_2). This plot displays a trade-off (black line) between gas permeability and permselectivity. This upper bound, represented in Figure 5 at T = 27 ºC, was developed by Rowe et al.[48] for the

CO_2/H_2 gas pair and was used to evaluate the performance of the prepared PIL–IL membranes at biohydrogen production conditions (T = 35 ºC and 100 kPa).

As it can be clearly seen from Figure 5, all PIL–IL membranes prepared in this work revealed CO_2/H_2 separation performances above the upper bound. An increment from 20 to 40 wt% of IL in the membrane not only promoted a significant increase in CO_2 permeability, but also increase the CO_2/H_2 permselectivity. Accordingly, the membrane composed of poly([Pyr_{11}][FSI]) and 40 wt% of [C_2mim][FSI] IL displayed the best CO_2/H_2 separation performance.

For comparison purposes, the PIL–IL membranes reported in our previous work, containing the $[TFSI]^-$ or $[C(CN)_3]^-$ anions, as well as literature data for other reported PIL–IL membranes are also included in Figure 5.[21] It can be observed that the CO_2/H_2 permselectivities obtained for both PIL FSI–40 IL FSI ($\alpha_{CO2/H2}$ = 8.9) and PIL TFSAM–40 IL TFSAM ($\alpha_{CO2/H2}$ = 7.2) membranes were found to be superior in comparison with those reported for PIL–IL membranes based on conventional $[TFSI]^-$ anion (PIL TFSI–40 [C_2mim][TFSI] ($\alpha_{CO2/H2}$ = 6.5) and PIL TFSI–60 [Pyr_{14}][TFSI] ($\alpha_{CO2/H2}$ = 6.3).[22] This means that the introduction of asymmetry in the IL' anion structure, as the case of $[TFSAM]^-$ anion, leads to enhanced CO_2/H_2 permselectivities, even when compared to PIL–IL membranes materials with higher amounts of incorporated IL containing the common $[TFSI]^-$ anion.

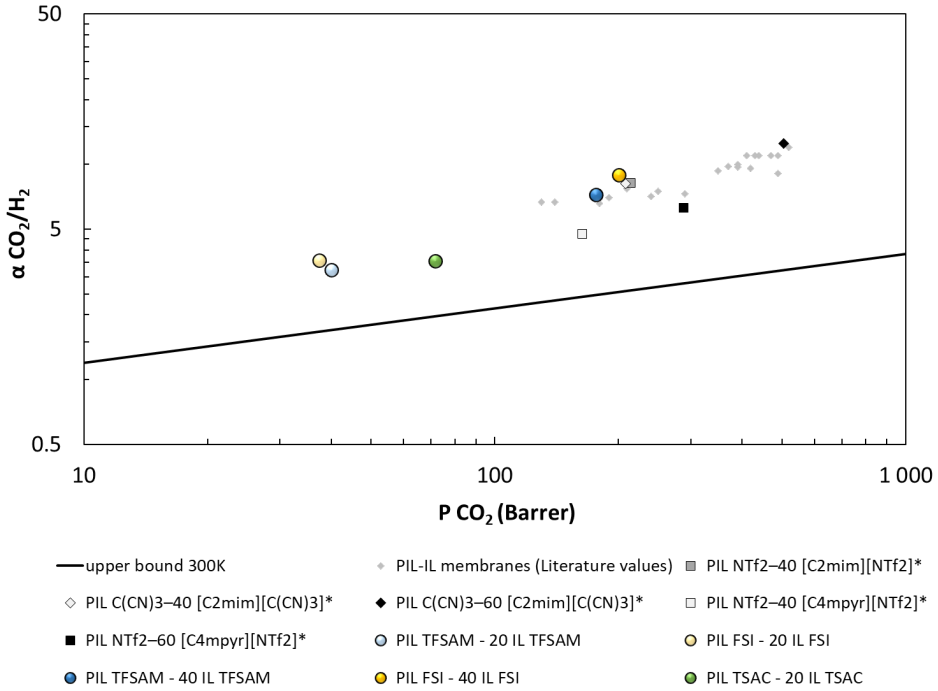

Figure 5. CO_2/H_2 separation performance of the PIL–IL membranes prepared in this work. The experimental error is within the data points. Data are plotted on a log–log scale and the upper bound at $T = 27$ ºC was adapted from Rowe et al.[48] Literature data points (♦) from other reported PIL–IL membranes are also displayed for comparison, as well as the PIL–IL composites reported in our previous work (*).[22]

CONCLUSIONS

Three poly(ionic liquid)s (PILs) were synthesized by ion exchange reaction between poly(diallyldimethylammonium) chloride and salts with $[TFSAM]^-$, $[TSAC]^-$ and $[FSI]^-$ anions. Further on, these PILs were used in the preparation of composite membranes with different amounts of ionic liquids (ILs) based on 1-methyl-3-ethylimidazolium ($[C_2mim]^+$) cation and bearing the same anion as respective PIL. The film-forming ability of composites was evaluated in terms of the maximum amount of neat IL that can be incorporated. All obtained neat ILs, PILs and PIL–IL membranes were characterized by a set of techniques (TGA, DSC, FT-IR and Raman) and their CO_2/H_2 and H_2/N_2 separation performances at bioH_2 production conditions (T = 35 ºC and p_{feed} = 1bar) were studied.

The FT-IR and Raman results showed an increase in the intensity of the IL's characteristic bands with increasing IL content in the composite. Regarding the thermal analysis, the onset weight loss temperatures for ILs and PILs were found to be strictly dependent on the anion's nature. The $[C_2mim][TSAC]$ showed the highest thermal stability (T_{onset} = 295 ^oC) among ILs, while for PILs the best result was achieved for poly($[Pyr_{11}][TFSAM]$) (T_{onset} = 280 ^oC). The DSC revealed the lower T_gs of PIL–IL composites compared to the corresponding neat PILs, demonstrating the plasticizing effect of IL's addition.

The CO_2, N_2 and H_2 permeabilities, diffusivities and solubilities were affected by the nature of the anion and the amount of the incorporated IL. All the prepared PIL–IL membranes revealed CO_2/H_2 separation performances above the upper bound. What is more, the CO_2/H_2 permselectivities of PIL TFSAM–40 IL TFSAM and PIL FSI–40 IL FSI membranes with 40 wt% of IL were found to be superior in comparison with those previously reported for composite membranes based on conventional $[TFSI]^-$ anion and containing 40 or even 60 wt% of IL. In order to better evaluate the CO_2/H_2 separation performance of the PIL–IL membranes here

presented, further studies regarding gas permeation tests with multi-component gas mixtures are currently in progress.

ASSOCIATED CONTENT

Supporting Information. FT-IR and Raman spectra of neat ILs and PILs and their composite membranes. TGA and DSC thermograms of studied ILs, PILs and PIL–IL membranes.

AUTHOR INFORMATION

***Corresponding Authors**

lilianasofi.carvalho@ehu.eus. Tel: +34 943 018018

isabel.marrucho@tecnico.ulisboa.pt. Fax: +351 21 8499242. Tel: +351 21 8413385

Notes

The authors declare no competing financial interest.

ACKNOWLEDGMENTS

Andreia S. L. Gouveia is grateful to FCT (Fundação para a Ciência e a Tecnologia) for her Doctoral (SFRH/BD/116600/2016) research grant. Liliana C. Tomé has received funding from the European Union's Horizon 2020 research and innovation programme under the Marie Sklodowska-Curie grant agreement No 745734. This work was supported by FCT through the project PTDC/CTM-POL/2676/2014. Centro de Química Estrutural acknowledges the financial support of Fundação para a Ciência e Tecnologia (UIDB/00100/2020). Elemental analysis and Raman spectroscopy were performed with the financial support from Ministry of Science and

Higher Education of the Russian Federation using the equipment of Center for molecular composition studies of INEOS RAS.

ABBREVIATIONS

Δp_d, variation of downstream pressure; Δp_i, pressure driving force; A, effective membrane surface area; bioH_2, biohydrogen; CO_2, carbon dioxide; D, diffusivity; H_2, hydrogen; H_2O, water; H_2S, hydrogen Sulfide; ILs, ionic liquids; J, steady-state gas flux; ℓ, membrane thickness; N_2, nitrogen; P, permeability; PILs, poly(ionic liquid)s; R, ideal gas law constant; S, solubility; t, time; T, temperature; V_p, permeate volume; α_{ij}, permselectivity; θ, time-lag parameter.

REFERENCES

1. Meher Kotay, S.; Das, D., Biohydrogen as a renewable energy resource—Prospects and potentials. *Int. J. Hydrogen Energy* **2008,** *33,* 258-263.

2. Merkel, T. C.; Zhou, M.; Baker, R. W., Carbon dioxide capture with membranes at an IGCC power plant. *J. Memb. Sci.* **2012,** *389,* 441-450.

3. Tomé, L. C.; Marrucho, I. M., Ionic liquid-based materials: a platform to design engineered CO2 separation membranes. *Chem. Soc. Rev.* **2016,** *45,* 2785-2824.

4. Scovazzo, P., Determination of the upper limits, benchmarks, and critical properties for gas separations using stabilized room temperature ionic liquid membranes (SILMs) for the purpose of guiding future research. *J. Memb. Sci.* **2009,** *343,* 199-211.

5. Gouveia, A. S. L.; Tome, L. C.; Lozinskaya, E. I.; Shaplov, A. S.; Vygodskii, Y. S.; Marrucho, I. M., Exploring the effect of fluorinated anions on the CO2/N2 separation of supported ionic liquid membranes. *Phys. Chem. Chem. Phys.* **2017,** *19,* 28876-28884.

6. Shaplov, A. S.; Lozinskaya, E. I.; Vlasov, P. S.; Morozova, S. M.; Antonov, D. Y.; Aubert, P. H.; Armand, M.; Vygodskii, Y. S., New family of highly conductive and low viscous ionic liquids with asymmetric 2,2,2-trifluoromethylsulfonyl-N-cyanoamide anion. *Electrochim. Acta* **2015,** *175,* 254-260.

7. Appetecchi, G. B.; Montanino, M.; Carewska, M.; Moreno, M.; Alessandrini, F.; Passerini, S., Chemical–physical properties of bis(perfluoroalkylsulfonyl)imide-based ionic liquids. *Electrochim. Acta* **2011,** *56,* 1300-1307.

8. Castiglione, F.; Moreno, M.; Raos, G.; Famulari, A.; Mele, A.; Appetecchi, G. B.; Passerini, S., Structural Organization and Transport Properties of Novel Pyrrolidinium-Based

Ionic Liquids with Perfluoroalkyl Sulfonylimide Anions. *J. Phys. Chem. B* **2009,** *113,* 10750-10759.

9. Matsumoto, H.; Kageyama, H.; Miyazaki, Y., Room temperature ionic liquids based on small aliphatic ammonium cations and asymmetric amide anions. *Chem. Commun.* **2002,** 1726-1727.

10. Reiter, J.; Jeremias, S.; Paillard, E.; Winter, M.; Passerini, S., Fluorosulfonyl-(trifluoromethanesulfonyl)imide ionic liquids with enhanced asymmetry. *Phys. Chem. Chem. Phys.* **2013,** *15,* 2565-2571.

11. Hajime, M.; Naohiro, T.; Tatsuya, U.; Seiji, T.; Hikari, S.; Kinji, A.; Kuniaki, T., *Chem. Lett.* **2008,** *37,* 1020-1021.

12. Bara, J.; Hatakeyama, E.; L. Gin, D.; D. Noble, R., Improving CO2 permeability in polymerized room□temperature ionic liquid gas separation membranes through the formation of a solid composite with a room□temperature ionic liquid. *Polym Advan Technol* **2008,** *19,* 1415-1420.

13. Tomé, L. C.; Gouveia, A. S. L.; Freire, C. S. R.; Mecerreyes, D.; Marrucho, I. M., Polymeric ionic liquid-based membranes: Influence of polycation variation on gas transport and CO2 selectivity properties. *J. Memb. Sci.* **2015,** *486,* 40-48.

14. Tomé, L. C.; Isik, M.; Freire, C. S. R.; Mecerreyes, D.; Marrucho, I. M., Novel pyrrolidinium-based polymeric ionic liquids with cyano counter-anions: High performance membrane materials for post-combustion CO2 separation. *J. Memb. Sci.* **2015,** *483,* 155-165.

15. Li, P.; Paul, D. R.; Chung, T.-S., High performance membranes based on ionic liquid polymers for CO2 separation from the flue gas. *Green Chem.* **2012,** *14,* 1052-1063.

16. Li, P.; Pramoda, K. P.; Chung, T.-S., CO2 Separation from Flue Gas Using Polyvinyl-(Room Temperature Ionic Liquid)–Room Temperature Ionic Liquid Composite Membranes. *Ind. Eng. Chem. Res.* **2011,** *50,* 9344-9353.

17. K. Carlisle, T.; F. Wiesenauer, E.; D. Nicodemus, G.; L. Gin, D.; D. Noble, R., Ideal CO2/Light Gas Separation Performance of Poly(vinylimidazolium) Membranes and Poly(vinylimidazolium)-Ionic Liquid Composite Films. *Ind. Eng. Chem. Res.* **2012,** *52,* 1023–1032.

18. Teodoro, R. M.; Tomé, L. C.; Mantione, D.; Mecerreyes, D.; Marrucho, I. M., Mixing poly(ionic liquid)s and ionic liquids with different cyano anions: Membrane forming ability and CO2/N2 separation properties. *J. Memb. Sci.* **2018,** *552,* 341-348.

19. Tomé, L. C.; Mecerreyes, D.; Freire, C. S. R.; Rebelo, L. P. N.; Marrucho, I. M., Pyrrolidinium-based polymeric ionic liquid materials: New perspectives for CO2 separation membranes. *J. Memb. Sci.* **2013,** *428,* 260-266.

20. Shaligram, S. V.; Wadgaonkar, P. P.; Kharul, U. K., Polybenzimidazole-based polymeric ionic liquids (PILs): Effects of 'substitution asymmetry' on CO2 permeation properties. *J. Memb. Sci.* **2015,** *493,* 403-413.

21. Carlisle, T. K.; Nicodemus, G. D.; Gin, D. L.; Noble, R. D., CO2/light gas separation performance of cross-linked poly(vinylimidazolium) gel membranes as a function of ionic liquid loading and cross-linker content. *J. Memb. Sci.* **2012,** *397–398,* 24-37.

22. Gouveia, A. S. L.; Ventaja, L.; Tomé, L. C.; Marrucho, I. M., Towards Biohydrogen Separation Using Poly(Ionic Liquid)/Ionic Liquid Composite Membranes. *Membranes* **2018,** *8,* 124.

23. Gouveia, A. S. L.; Bernardes, C. E. S.; Tome, L. C.; Lozinskaya, E. I.; Vygodskii, Y. S.; Shaplov, A. S.; Lopes, J. N. C.; Marrucho, I. M., Ionic liquids with anions based on fluorosulfonyl derivatives: from asymmetrical substitutions to a consistent force field model. *Phys. Chem. Chem. Phys.* **2017,** *19,* 29617-29624.

24. Pont, A.-L.; Marcilla, R.; De Meatza, I.; Grande, H.; Mecerreyes, D., Pyrrolidinium-based polymeric ionic liquids as mechanically and electrochemically stable polymer electrolytes. *J. Power Sources* **2009,** *188,* 558-563.

25. Brinkkötter, M.; Lozinskaya, E. I.; Ponkratov, D. O.; Vlasov, P. S.; Rosenwinkel, M. P.; Malyshkina, I. A.; Vygodskii, Y.; Shaplov, A. S.; Schönhoff, M., Influence of anion structure on ion dynamics in polymer gel electrolytes composed of poly(ionic liquid), ionic liquid and Li salt. *Electrochim. Acta* **2017,** *237,* 237-247.

26. Appetecchi, G. B.; Kim, G. T.; Montanino, M.; Carewska, M.; Marcilla, R.; Mecerreyes, D.; De Meatza, I., Ternary polymer electrolytes containing pyrrolidinium-based polymeric ionic liquids for lithium batteries. *J. Power Sources* **2010,** *195,* 3668-3675.

27. Papatheodorou, G. N., Kalampounias, A. G. and Yannopoulos, S. N. , In *Raman Spectroscopy of High Temperature Melts in Molten Salts and Ionic Liquids*, Seddon, M. G. E. a. K. R., Ed. 2012; pp 301-340.

28. Jin, L.; Nairn, K. M.; Forsyth, C. M.; Seeber, A. J.; MacFarlane, D. R.; Howlett, P. C.; Forsyth, M.; Pringle, J. M., Structure and Transport Properties of a Plastic Crystal Ion

Conductor: Diethyl(methyl)(isobutyl)phosphonium Hexafluorophosphate. *J. Am. Chem. Soc.* **2012,** *134,* 9688-9697.

29. Gómez, E.; Calvar, N.; Domínguez, Á., Thermal Behaviour of Pure Ionic Liquids In *Ionic Liquids - Current State of the Art*, Handy, S., Ed. IntechOpen, 2015; pp 200-228.

30. Wijmans, J. G.; Baker, R. W., The solution-diffusion model: a review. *J. Memb. Sci.* **1995,** *107,* 1-21.

31. Matteucci, S.; Yampolskii, Y.; Freeman, B. D.; Pinnau, I., Transport of Gases and Vapors in Glassy and Rubbery Polymers. In *Materials Science of Membranes for Gas and Vapor Separation*, John Wiley & Sons, Ltd: 2006; pp 1-47.

32. Rutherford, S. W.; Do, D. D., Review of time lag permeation technique as a method for characterisation of porous media and membranes. *Adsorption* **1997,** *3,* 283-312.

33. Kiefer, J.; Fries, J.; Leipertz, A., Experimental vibrational study of imidazolium-based ionic liquids: Raman and infrared spectra of 1-ethyl-3-methylimidazolium bis(trifluoromethylsulfonyl)imide and 1-ethyl-3-methylimidazolium ethylsulfate. *Appl Spectrosc* **2007,** *61,* 1306-11.

34. Moumene, T.; Belarbi, E. H.; Haddad, B.; Villemin, D.; Abbas, O.; Khelifa, B.; Bresson, S., Vibrational spectroscopic study of ionic liquids: Comparison between monocationic and dicationic imidazolium ionic liquids. *J. Mol. Struct.* **2014,** *1065-1066,* 86-92.

35. Na, R.; Su, C.-W.; Su, Y.-H.; Chen, Y.-C.; Chen, Y.-M.; Wang, G.; Teng, H., Solvent-free synthesis of an ionic liquid integrated ether-abundant polymer as a solid electrolyte for flexible electric double-layer capacitors. *J. Mater. Chem. A* **2017,** *5,* 19703-19713.

36. Paschoal, V. H.; Faria, L. F. O.; Ribeiro, M. C. C., Vibrational Spectroscopy of Ionic Liquids. *Chem. Rev.* **2017,** *117,* 7053-7112.

37. Yunis, R.; Girard, G. M. A.; Wang, X.; Zhu, H.; Bhattacharyya, A. J.; Howlett, P.; MacFarlane, D. R.; Forsyth, M., The anion effect in ternary electrolyte systems using poly(diallyldimethylammonium) and phosphonium-based ionic liquid with high lithium salt concentration. *Solid State Ionics* **2018,** *327,* 83-92.

38. Huang, J.; Hollenkamp, A. F., Thermal Behavior of Ionic Liquids Containing the FSI Anion and the Li+ Cation. *J. Phys. Chem. C* **2010,** *114,* 21840-21847.

39. Fujii, K.; Seki, S.; Fukuda, S.; Kanzaki, R.; Takamuku, T.; Umebayashi, Y.; Ishiguro, S.-i., Anion Conformation of Low-Viscosity Room-Temperature Ionic Liquid 1-Ethyl-3-methylimidazolium Bis(fluorosulfonyl) Imide. *J. Phys. Chem. B* **2007,** *111,* 12829-12833.

40. Moumene, T.; Belarbi, E. H.; Haddad, B.; Villemin, D.; Abbas, O.; Khelifa, B.; Bresson, S., Study of imidazolium dicationic ionic liquids by Raman and FTIR spectroscopies: The effect of the nature of the anion. *J. Mol. Struct.* **2015,** *1083,* 179-186.

41. Noack, K.; Schulz, P. S.; Paape, N.; Kiefer, J.; Wasserscheid, P.; Leipertz, A., The role of the C2 position in interionic interactions of imidazolium based ionic liquids: a vibrational and NMR spectroscopic study. *Phys. Chem. Chem. Phys.* **2010,** *12,* 14153-14161.

42. Yuan, J.; Mecerreyes, D.; Antonietti, M., Poly(ionic liquid)s: An update. *Prog. Polym. Sci.* **2013,** *38,* 1009-1036.

43. Wang, X.; Zhu, H.; Girard, Gaetan M. A.; Yunis, R.; MacFarlane, D. R.; Mecerreyes, D.; Bhattacharyya, A. J.; Howlett, P. C.; Forsyth, M., Preparation and characterization of gel polymer electrolytes using poly(ionic liquids) and high lithium salt concentration ionic liquids. *J. Mater. Chem. A* **2017,** *5,* 23844-23852.

44. Scott, M. P.; Brazel, C. S.; Benton, M. G.; Mays, J. W.; Holbrey, J. D.; Rogers, R. D., Application of ionic liquids as plasticizers for poly(methyl methacrylate). *Chem. Commun.* **2002,** 1370-1371.

45. Zain, N. F.; Zainal, N.; Mohamed, N. S., The influences of ionic liquid to the properties of poly(ethylmethacrylate) based electrolyte. *Physica Scripta* **2015,** *90,* 015702- 015709.

46. Elamin, K.; Shojaatalhosseini, M.; Danyliv, O.; Martinelli, A.; Swenson, J., Conduction mechanism in polymeric membranes based on PEO or PVdF-HFP and containing a piperidinium ionic liquid. *Electrochim. Acta* **2019,** *299,* 979-986.

47. Wang, S.; Li, X.; Wu, H.; Tian, Z.; Xin, Q.; He, G.; Peng, D.; Chen, S.; Yin, Y.; Jiang, Z.; Guiver, M. D., Advances in high permeability polymer-based membrane materials for CO2 separations. *Energy Environ. Sci.* **2016,** *9,* 1863-1890.

48. Rowe, B. W.; Robeson, L. M.; Freeman, B. D.; Paul, D. R., Influence of temperature on the upper bound: Theoretical considerations and comparison with experimental results. *J. Memb. Sci.* **2010,** *360,* 58-69.

"For Table of Contents Use Only"

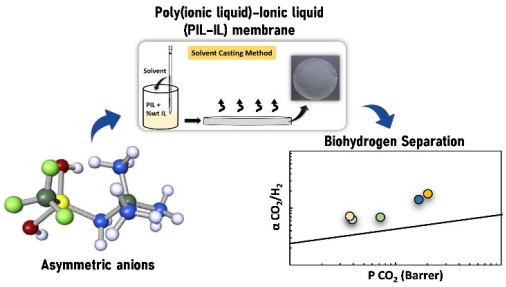

Introduction of asymmetry in IL' anion structure can be an attractive strategy to tune gas permeation properties of PIL-IL composites for important energy applications.